Journal of Catalysis **184,** 262–267 (1999)
Article ID jcat.1999.2423, available online at http://www.idealibrary.com on IDEAL®

Oligomerization of Hex-1-ene over Acidic Aluminosilicate Zeolites, MCM-41, and Silica-Alumina Co-gel Catalysts: A Comparative Study

Jérôme P. G. Pater, Pierre A. Jacobs, and Johan A. Martens

Centrum voor Oppervlaktechemie en Katalyse, Department Interfasechemie, K.U. Leuven, Kardinaal Mercierlaan 92, B-3001 Heverlee, Belgium

Received November 9, 1998; revised January 11, 1999; accepted January 11, 1999

Hex-1-ene in octane solvent was oligomerized in a down-flow tubular reactor holding a fixed catalyst bed at temperatures of 80–300°C and a pressure of 5 MPa. Ultrastable Y (US-Y), hydrogen beta, and MCM-22 zeolites, MCM-41, silica–alumina and silica–magnesia co-gels, and γ-alumina were evaluated as catalysts. The reaction products obtained are composed of hexene dimers and trimers, cracked products, C_6 alkanes, and isohexenes. The catalytic activity of the mesoporous silica–alumina co-gels and MCM-41 is very similar to that of beta, MCM-22, and US-Y zeolites. The oligomerization process occurs in the mesopores and on the exterior surfaces of the zeolite crystals. In the micropores of zeolite beta and US-Y, the hexenes undergo dimerization-cracking reactions generating isohexenes and cracked products. In MCM-22, having narrower micropores, these cracking reactions are suppressed. MCM-22, MCM-41, and silica–alumina co-gels lacking microporosity are the most selective hexene dimerization catalysts. © 1999 Academic Press

Key Words: **oligomerization; hexenes; acid catalysis; mesoporous catalysts; MCM-22; MCM-41; zeolite beta; ultrastable zeolite Y.**

1. INTRODUCTION

Oligomerization is applied to convert light alkenes into fuels. A typical example is the acid catalyzed oligomerization of $C_3^=$-$C_4^=$ alkenes produced by FCC (fluid catalytic cracking) into gasoline, distillate, or lubricants (1–4). Phosphoric acid on Kieselguhr is a popular heterogeneous alkene oligomerization catalyst developed by Ipatieff *et al.* (2). A drawback of the supported phosphoric acid catalyst is the critical hydration level of the feedstock and its deactivation by deposition of heavy oligomers and tars that tend to glue the catalyst particles together complicating spent catalyst removal (3). The invention of shape-selective zeolites and, especially, of ZSM-5 led to the development of the MOGD processes (mobil olefins to gasoline and distillate) (5–9). The distillate to gasoline ratio can be adjusted by tuning the reaction conditions with pressures up to 10 MPa and temperatures above 463 K favoring MOD. Over the ZSM-5 catalyst, the alkenes undergo multiple oligomerization and recracking steps. Alkenes with six and more carbon atoms are first cracked and the fragments subsequently copolymerized, a mechanism designated as "hetero-oligomerization" (10). The skeletal branching of the products is therefore independent of the nature of the feedstock as demonstrated with alkenes from C_2 to C_{10} (11). In the oligomers there is typically one methylbranching per five carbons in a chain (7). The advantage of ZSM-5 compared to zeolites with wider pores is its relatively slow deactivation, owing to the steric suppression of the formation of bulky coke precursor molecules inside its micropores (5). The low acid site density is another factor explaining the slow deactivation of ZSM-5 (12). Nevertheless, there is deactivation proceeding through the formation of high molecular weight products on the external surfaces blocking pore mouths (13). This deactivation is an important obstacle in the MOG and MOD processes, necessitating special reactor design with continuous catalyst regeneration (14).

In a previous paper (15), we investigated the possibility of oligomerizing hex-1-ene according to a true oligomerization mechanism. It was found that ultrastable Y (US-Y) zeolite and H-beidellite catalyze hex-1-ene dimerization and have good time-on-stream stability, provided the oligomerization process is run in the liquid phase in presence of *n*-alkane solvent. In the present paper, we used those optimized reaction conditions for a comparative study of hydrogen zeolites, MCM-41, and mixed oxide types of catalysts, representing a broad range of pore sizes and acidities. We made an attempt to identify the critical catalyst parameters for obtaining a true oligomerization of this type of alkene feedstock.

2. EXPERIMENTAL

The US-Y zeolite powder sample was from PQ (Code name CBV-720) and the H-beta zeolite from Süd-Chemie. MCM-22 was synthesized according to (16), calcined, and ammonium exchanged. The aluminosilicate MCM-41 was synthesized according to (17). The sample was calcined in a muffle furnace at 550°C for 10 h to remove the organic template and subsequently ammonium exchanged.

0021-9517/99 $30.00

TABLE 1

Physico-Chemical Characteristics of the Catalysts

Catalysts	Specific surface area ($m^2 \cdot g^{-1}$) BET	Specific surface area ($m^2 \cdot g^{-1}$) Outside micropores	Micropore volume ($cm^3 \cdot g^{-1}$)	Mesopore volume[a] ($cm^3 \cdot g^{-1}$)	Si/Al atomic ratio
US-Y	658	108	0.253	0.122	13[b]
Beta	583	168	0.190	0.180	12.5[b]
MCM-22	442	106	0.155	0.103	21[c]
MCM-41	900	922	0	0.730	29[c]
SiAl(1)	385	374	0	0.739	6[b]
SiAl(2)	499[b]	n.d.[d]	0[b]	n.d.	140[b]
SiAl(3)	300[b]	n.d.	0[b]	n.d.	$1.3\ 10^{-3}$[b]
Silica–Mg	334[b]	n.d.	0[b]	n.d.	—
γ-Alumina	150[b]	n.d.	0[b]	n.d.	—

[a] Pore diameters from 2 to 10 nm.
[b] According to the manufacturer.
[c] According to the original literature.
[d] Not determined.

The following co-gels were from Grace: silica–alumina type 13/110, containing 13 wt% of Al_2O_3, denoted as SiAl(1), a surface-enriched co-gel with an alumina content of 0.6 wt%, denoted as SiAl(2), and silica–magnesia containing 1 wt% of MgO. The silicoaluminate Siralox 1.5/200, containing 1.5 wt% of SiO_2 and denoted as SiAl(3) and the γ-alumina Puralox NWa-155 were from Condea.

The specific surface area and the porosity were characterized based on nitrogen physisorption isotherms recorded at 77 K using an Omnisorp instrument Series 360 from Coulter (Table 1). The specific surface area was calculated according to the BET method (18). The specific surface area in mesopores and the micropore volume were calculated using *t*-plots (19). The mesopore volume assuming an open-ended nonintersection cylindrical pore system was calculated according to the BJH method (20).

Catalyst powders were compressed into wafers that were crushed and sieved to obtain particles with diameters of 250–500 μm. The catalytic experiments were carried out in a downstream fixed-bed reactor tube holding 3 g of catalyst pellets and mounted in a tubular furnace. The dead volume inside the reactor tube was filled with glass beads with the same diameter as the catalyst particles. The catalyst temperature was monitored with an axially positioned thermocouple inside the bed. The catalysts were activated *in situ* in the reactor tube by a calcination under flowing oxygen (3 $cm^3\ s^{-1}\ g^{-1}$) for 5 h at 450°C. The catalyst was subsequently cooled to 80°C and solvent was pumped through the reactor. The feedstock was composed of 30 wt% of hex-1-ene (>97%, Acros) mixed with 70 wt% octane (>99%, Acros). The feedstock mixture was prepared by mixing pure compounds in a pressure vessel equipped with a stirrer. Heptane was used as an internal standard. The liquid feedstock was delivered to the reactor by means of a mass flow controller for liquids (Rosemount/Brooks Instruments B. V., type 5881) at a flow rate of 5 $g \cdot h^{-1}$, corresponding to a WHSV of 0.5 h^{-1} on hex-1-ene basis. The pressure in the reactor was kept at 5 MPa by means of a back-pressure regulator.

The reaction products were sampled at high pressure using a sampling valve with an internal volume of 0.1 μl, located upstream of the back-pressure regulator, and transferred by means of a heated transfer line to a gaschromatograph (HP 5890 Series II) equipped with a fused silica WCOT column (CP-SiL 5 CB from Chrompack; length of 50 m; internal diameter of 0.32 mm; film thickness of 5.0 μm) and FID detector.

Product sampling was done after 1.5 h of operation of the reactor at a fixed temperature. The reaction temperature was increased to the next temperature level immediately after a product sampling.

Liquid product fractions were collected in a gas–liquid separator at 15°C and atmospheric pressure. The skeletal branching of the oligomers was analyzed using the same type of gas-chromatograph as for on-line analysis, additionally equipped with a catalytic hydrogenation module (modified TCT injection system from Chrompack using a Pd catalyst at 180°C).

3. RESULTS

On all the catalysts investigated, hex-1-ene was rapidly isomerized into *t*-hex-2-ene and *c*-hex-2-ene. For example, at temperatures above 100°C, the composition of the linear hexene product fraction was 46% *t*-hex-2-ene, 38% *c*-hex-2-ene, and 16% hex-1-ene irrespective of the catalyst, reflecting the thermodynamic equilibrium distribution of these isomers (7). Double bond isomerization is known to be a facile reaction (21). The linear $C_6^=$ compounds were lumped and considered later on as unconverted "hexene". The hexene conversion obtained with the different catalysts at increasing reaction temperatures is traced in Fig. 1. With

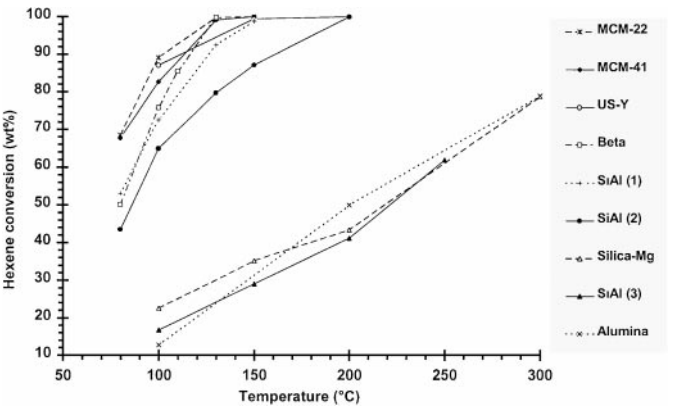

FIG. 1. Hexene conversion against reaction temperature obtained on the different catalysts. Time-on-stream at each temperature: 1.5 h.

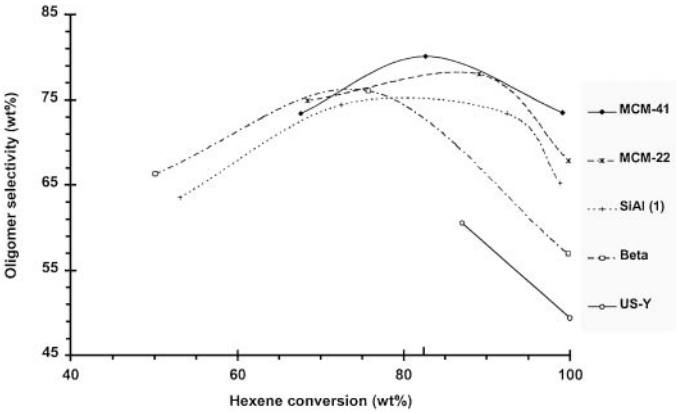

FIG. 2. Oligomer selectivity against hexene conversion (Experiments of Fig. 1).

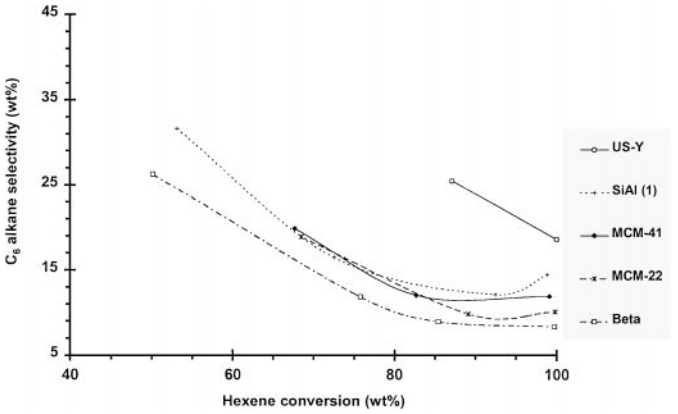

FIG. 4. C_6 alkane selectivity against hexene conversion (Experiments of Fig. 1).

respect to catalytic activity, the catalysts can be subdivided into two groups. On MCM-22, MCM-41, US-Y, beta, and SiAl(1), high hexene conversions were obtained at moderate temperatures. Almost complete hexene conversions were reached around 130°C on MCM-41, MCM-22, and beta, and at ca. 150°C on SiAl(1) and US-Y. SiAl(2) was somewhat less active, but reached complete hexene conversion at 200°C. The γ-alumina, SiAl(3), and silica–magnesia co-gel are much less active. The hexene conversions obtained with these three catalysts did not exceed 60%, even at temperatures as high as 300°C.

The most active catalysts (SiAl(1), MCM-41, beta, MCM-22, and US-Y) showed very little deactivation when they were run at a constant temperature for 12 h or with temperature increments. Under these low temperature, liquid phase operation conditions, the selectivity patterns are strongly influenced by the catalyst aging.

With all catalysts, the reaction products were composed of compounds with carbon numbers from 3 to 12, and 18. The reaction products were grouped as follows: (i) oligomers, which are the fractions with carbon numbers 12 and 18 and in which C_{12} products represented generally more than 95 wt%; (ii) cracked products having carbon numbers from 3 to 5 and 7 to 11; (iii) C_6 saturates, which are C_6 alkanes present in significant amounts in the C_6 fraction; and (iv) isohexenes. It has to be mentioned that the cracked product fractions contained some minor amounts of saturates as well, but given the low selectivity for cracking, no further attention was paid to saturates formation in those fractions. The selectivity for oligomers, cracked products, C_6 saturates and C_6 isoalkenes obtained with the most active catalysts are presented in Figs. 2–5, respectively.

On all catalysts, the oligomerization selectivity goes through a maximum (Fig. 2). At hexene conversions exceeding 80%, the oligomerization selectivity decreases in the following catalyst order:

$$\text{MCM-41} > \text{MCM-22} > \text{SiAl(1)} > \text{beta} > \text{US-Y}. \quad [1]$$

Cracking of oligomers and the formation of C_6 saturates

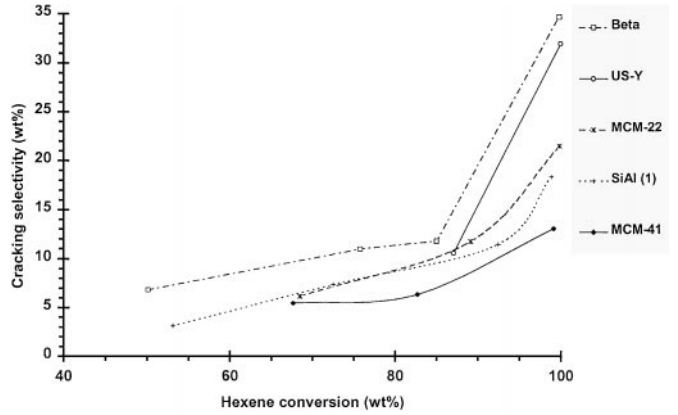

FIG. 3. Cracked product selectivity against hexene conversion (Experiments of Fig. 1).

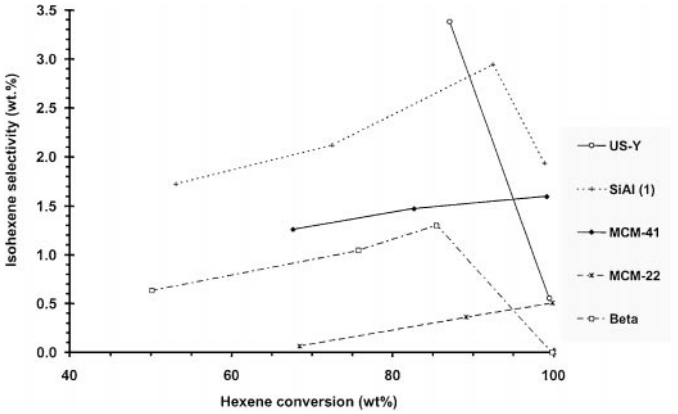

FIG. 5. Isohexene selectivity against hexene conversion (Experiments of Fig. 1).

are the main side reactions (Figs. 3 and 4). The cracking selectivity increases with increasing conversion, especially in the range from 90 to 100% conversion (Fig. 3). At those high conversions, the cracking selectivity decreases in the catalyst order:

$$\text{Beta} > \text{US-Y} > \text{MCM-22} > \text{SiAl(1)} > \text{MCM-41}. \quad [2]$$

On all catalysts, the selectivity for C_6 saturates formation decreases with increasing hexene conversion (Fig. 4). Since the carbon balance evaluated with the internal standard did not show a large deficiency, the hydrogen deficient molecules must be contained in the cracked product or oligomer product fractions, but could not be identified. The C_6 saturates formation is dependent on the catalyst. The selectivity for C_6 saturates formation decreases in the following catalyst order:

$$\text{US-Y} \gg \text{SiAl(1)} \approx \text{MCM-41} \approx \text{MCM-22} > \text{beta}. \quad [3]$$

Branched hexenes including 2-methyl-pent-2-ene, 3-methyl-trans-pent-2-ene, and 3-methyl-cis-pent-2-ene were formed at high hexene conversions (Fig. 5).

The distribution of the dimer product fraction according to branching degree at increasing hexene conversions obtained on the different catalysts is reported in Figs. 6–8. The majority of dimers are dibranched (Fig. 7). Dibranched and monobranched dimers appear as primary products (Figs. 6 and 7) and the tribranched dimers as secondary products (Fig. 8).

4. DISCUSSION

The collection of catalysts used for this study represents a wide variation of textures (Table 1). The zeolites US-Y, beta, and MCM-22 have large micropore volumes located inside the crystals. The micropore windows in zeolite beta and Y are circumscribed by 12 rings of oxygen atoms; MCM-22 has a complex micropore structure with 10-ring openings (22). The mesopore volume in the zeolites is present either inside the crystals as a result of a dealumination treatment (US-Y) or between individual crystallites of a polycrystalline material (beta and MCM-22). The SiAl co-gels do not contain micropores (Table 1). The MCM-41 material used in this study is a mesoporous silica–alumina with cylindrical pores having free diameters of ca. 4 nm (23). The mesopore volume of SiAl(1) is very similar to that of MCM-41, but the mesopores are wider and the distribution broader.

Alkene oligomerization is catalyzed by Brønsted acid sites (24). The catalysts used in this study represent a variety of acid strengths. Aluminosilicate zeolites possess much stronger Brønsted acid sites compared to amorphous aluminosilicates (25). The Brønsted acid strength in MCM-41 is comparable to that of amorphous silica–alumina (26). The screening of catalysts (Fig. 1) reveals that the Brønsted acidity of amorphous aluminosilicates (MCM-41, SiAl(1))

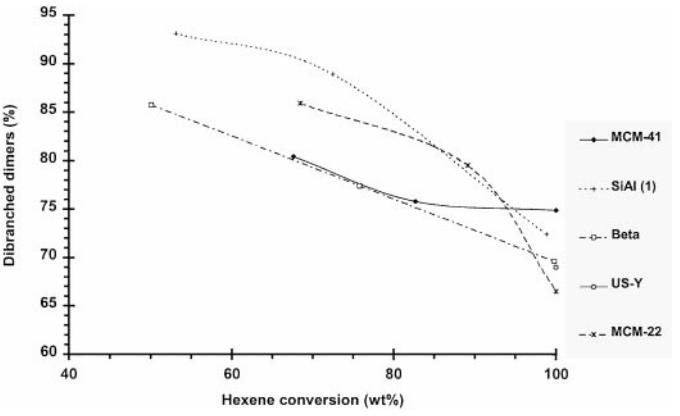

FIG. 7. Evolution of the content of dibranched isomers in the C_{12} fraction with increasing hexene conversion (Experiments of Fig. 1).

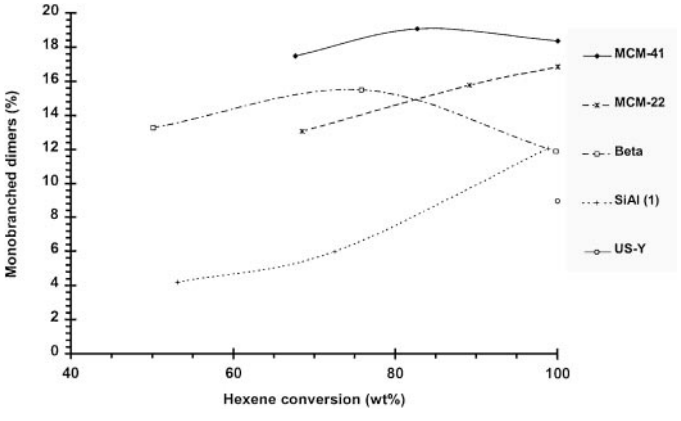

FIG. 6. Evolution of the content of monobranched isomers in the C_{12} fraction with increasing hexene conversion (Experiments of Fig. 1).

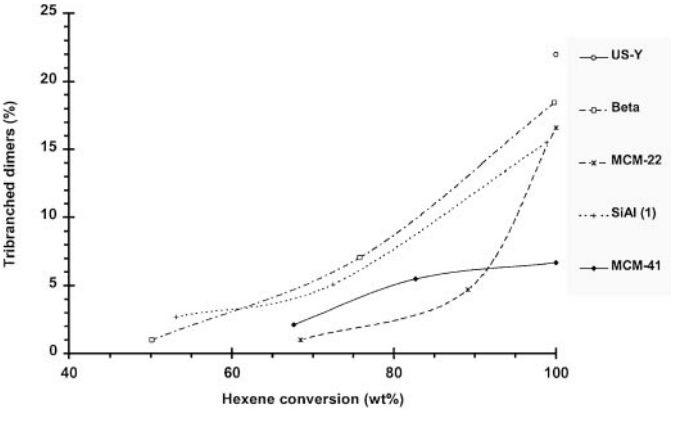

FIG. 8. Evolution of the content of tribranched isomers in the C_{12} fraction with increasing hexene conversion (Experiments of Fig. 1).

is sufficient to catalyze hexene oligomerization. The less active catalysts including γ-alumina, the silica doped alumina, and the silica–magnesia co-gel are the weakest solid Brønsted acids among the materials tested and do not possess sufficient Brønsted acidity. Within one family of materials, the activity is dependent on the number of acid sites. The SiAl(2) material contains less aluminium and less Brønsted acid sites compared to SiAl(1) and is less active. Brønsted acidity is, however, not the key parameter governing the catalytic activity in hexene oligomerization. MCM-41 and SiAl(1) exhibit a catalytic activity that is very similar to that of high-silica aluminosilicate zeolites beta and MCM-22, having much stronger acid sites in their micropores. Given the similar activity and selectivity, it seems that micropores are not essential to the oligomerization process and that the oligomerization reactions proceed on the large external surface areas (beta, MCM-22) or in the mesopores (US-Y) of the zeolites.

The dimerization of hexenes on a Brønsted acid site proceeds over bulky transition states, in which a C–C bond is created between a positively charged carbon atom of a hexyl cation and a carbon atom of the double bond of a hexene molecule (Scheme 1). Monobranched C_{12} skeletons can be obtained from reactions of hex-1-ene and a hex-2-yl or hex-3-yl cation, and dibranched C_{12} skeletons from reactions of hex-2-ene and hex-3-ene with hex-2-yl and hex-3-yl cations. In the dibranched dimers, the two branchings are always at vicinal carbon positions near the center of the main chain. Since the hex-1-ene fed to the reactor is rapidly isomerized into hex-2-ene and hex-3-ene, the dimers are mainly dibranched (Fig. 7). Monobranched dimers are also primary products, but formed less abundantly (Fig. 6).

Tribranched dimers cannot be directly obtained as primary products from linear hexenes. The formation of tribranched dimers is possible starting from an isohexyl cation and a linear hexene molecule or else from an unbranched hexyl cation and an isohexene molecule (Scheme 1).

The formation of tribranched C_{12} isomers (Fig. 8) can be explained by this type of dimerizations or else by a rearrangement of dibranched isomers.

In isomerization and hydrocracking of heptane on zeolite Pt/H-beta, dimerization reactions of heptene reaction intermediates and their cracking were invoked to explain skeletal isomerization and cracking patterns (27). At reaction temperatures above 200°C, dimerization–cracking of heptenes is a fast reaction on zeolite beta, generating branched isoheptenes in parallel with products with other carbon numbers. These oligomerization–recracking processes occur inside the zeolite beta crystals at the channel intersections and are subjected to molecular shape selectivity (27). In the present experiments with zeolite beta, cracking and skeletal branching of hexenes are also parallel reactions (Fig. 9), suggesting the occurrence of the same dimerization–cracking mechanisms. At these low temperatures, these reactions are much slower and appear as undesired side-reactions. In dimerization–cracking, US-Y zeolites are less active than beta zeolites (28). In the present work, the US-Y zeolite is also less selective to cracking and $C_6^=$ skeletal branching compared to beta (Figs. 3 and 5).

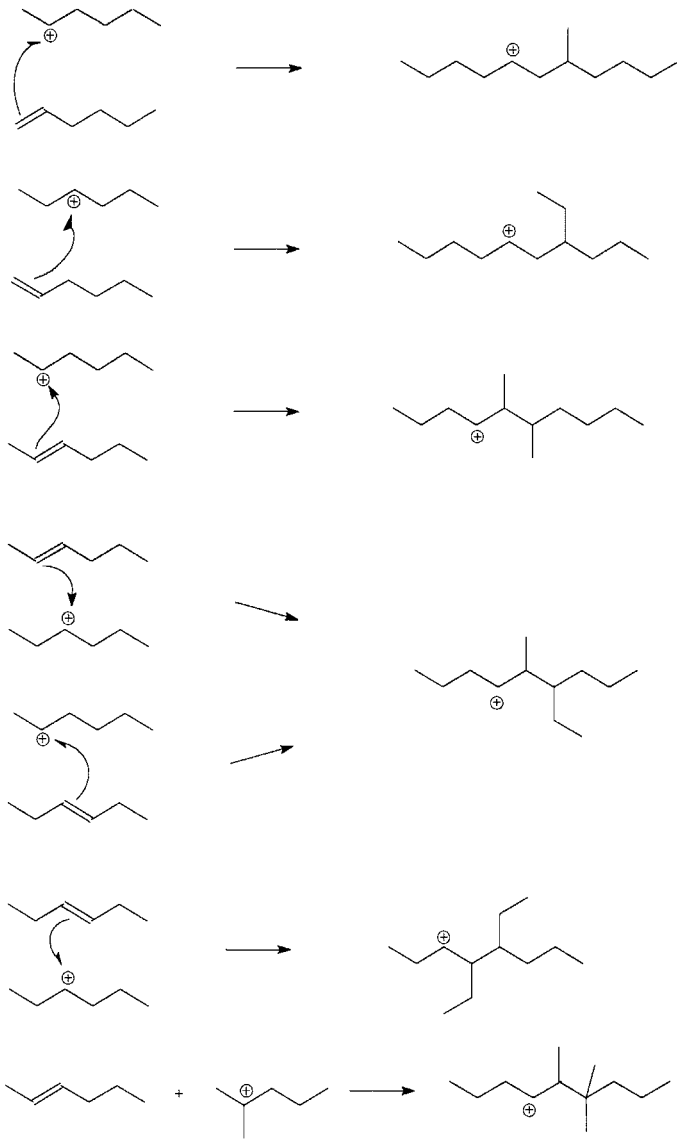

SCHEME 1. Examples of alkylation reactions leading to the formation of monobranched, dibranched, and tribranched C_{12} products.

MCM-22 has a complex micropore structure in which the strongest Brønsted acid sites are present in tubular 10-ring channel segments (29). The cracking selectivity of MCM-22 is lower than in beta and US-Y (Fig. 3). This is likely due to a shape selective suppression of the dimerization–cracking reactions in this narrow tubular pore system. With respect to cracking, the behavior of MCM-22 approaches that of the MCM-41 and SiAl(1) materials that do not contain micropores (Fig. 3).

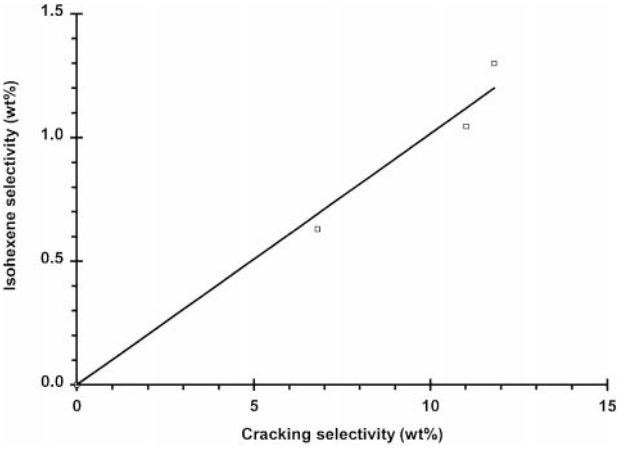

FIG. 9. Isohexene selectivity versus cracking selectivity on zeolite beta (Data from Figs. 3 and 5).

The formation of C_6 alkanes is a primary reaction (Fig. 4) and can be explained by hydride transfer to a C_6 alkylcarbenium ion formed by adsorption of hexene on a Brønsted acid site (30).

Ultrastable Y zeolite is known to be a very effective hydrogen transfer catalyst, a property that is exploited in the fluid catalytic cracking process (31). Zeolite beta is a less efficient hydrogen transfer catalyst (32). In hexene oligomerization, the hydrogen transfer activity of MCM-41, MCM-22, and SiAl(1) are intermediate between US-Y and beta (Fig. 4).

5. CONCLUSIONS

Mesoporous aluminosilicate catalysts with a high specific surface area are effective catalysts for hexene dimerization. A similar catalytic activity is developed by small zeolite crystals exposing more than 100 $m^2 \cdot g^{-1}$ of exterior specific surface area (zeolite beta, MCM-22) or in intracrystalline mesopores (US-Y). Catalytic activity in the zeolite micropores is responsible for undesired side reactions such as cracking (zeolite beta) and hydrogen transfer (US-Y). These side reactions are suppressed by molecular shape selectivity in MCM-22 zeolites having narrow 10-ring tubular channels.

ACKNOWLEDGMENTS

This work has been sponsored by Total Raffinage Distribution S. A. Stimulating discussions with J. M. Colin, R. Loutaty, A. Pantazidis, G. Szabo (from CERT TOTAL, Harfleur-France), and C. Naccache (from IRC, Villeurbanne-France) were greatly appreciated.

REFERENCES

1. Carey, J. S., *Refin. Natur. Gas. Mfr.* **15**, 549 (1936).
2. Ipatieff, V. N., Corson, B. B., and Egloff, G., *Ind. Eng. Chem.* **27**, 1077 (1935).
3. Jones, E. K., *in* "Advances in Catalysis" (W. G. Frankenburg, and V. I. Komarewsky, Eds.), Vol. 8, p. 219. Academic Press, San Diego, 1956.
4. Oblad, A. G., Mills, G. A., and Heinemann, H., *in* "Catalysis" (P. H. Emmett, Ed.), Vol. 6, p. 341. 1958.
5. van den Berg, J. P., Wolthuizen, J. P., and van Hooff, J. H. C., *J. Catal.* **80**, 139 (1983).
6. van den Berg, J. P., Wolthuizen, J. P., Clague, A. D. H., Hays, G. R., Huis, R., and van Hooff, J. H. C., *J. Catal.* **80**, 130 (1983).
7. Quann, R. J., Green, L. A., Tabak, S. A., and Krambeck, F. J., *Ind. Eng. Chem. Res.* **27**, 565 (1988).
8. Gricus Kofke, T. J., and Gorte, R. J., *J. Catal.* **115**, 223 (1989).
9. Sealy, S. J., Fraser, D. M., Möller, K. P., and O'Connor, C. T., *Chem. Eng. Sci.* **49**, 3307 (1994).
10. Langlois, G. E., *Ind. Eng. Chem.* **45**, 7, 1470 (1953).
11. Garwood, W. E., *in* "Intrazeolite Chemistry" (D. Stucky, and F. G. Dwyer, Eds.), A.C.S. Symp. Ser. Vol. 218, p. 383. Amer. Chem. Soc., Washington, DC., 1983.
12. Guisnet, M., and Magnoux, P., *in* "Zeolites Microporous Solids: Synthesis, Structure and Reactivity" (E. G. Derouane, *et. al.*, Eds.), p. 437. Kluwer Academic, Dordrecht/Norwell, MA, 1992.
13. Froment, G. F., De Meyer, J., and Derouane, E. G., *J. Catal.* **124**, 391 (1980).
14. Harandi, EPA 375 286 (1990).
15. Pater, J. P. G., Martens, J. A., and Jacobs, P. A., *J. Catal.* **179**, 477 (1998).
16. Rubin, M. K., and Chu, P., U.S. Patent 4,954,325, 1990.
17. Chen, C. Y., Li, H. X., and Davis, M. E., *Micropor. Mater.* **2**, 17 (1993).
18. Brunauer, S., Emmett, P. H., and Teller, E., *J. Amer. Chem. Soc.* **60**, 309 (1938).
19. Lippens, B. C., and de Boer, J. H., *J. Catal.* **4**, 319 (1965).
20. Barrett, E. P., Joyner, L. G., and Halenda, P. H., *J. Amer. Chem. Soc.* **73**, 373 (1951).
21. Jacobs, P. A., "Carboniogenic Activity of Zeolites." Elsevier, Amsterdam, 1977.
22. Leonowicz, M. E., Lawton, J. A., Lawton, S. L., and Rubin, M. K., *Science* **264**, 1910 (1994).
23. Chen, C.-Y., Li, H.-X., and Davis, M. E., *Micropor. Mater.* **2**, 17 (1993).
24. Skupinska, J., *Chem. Rev.* **91**, 613 (1991).
25. Kazansky, V. B., Mortier, W. J., Baekelandt, B. G., and Lievens, J. L., *J. Mol. Catal.* **83**, 175 (1993).
26. Llewellyn, P. L., Ciesla, U., Decher, H., Stadler, R., Schüth, F., and Unger, K. K., *Stud. Surf. Sci. Catal.* **84**, 2013 (1994).
27. Blomsma, E., Martens, J. A., and Jacobs, P. A., *J. Catal.* **155**, 141 (1995).
28. Blomsma, E., Martens, J. A., and Jacobs, P. A., *J. Catal.* **159**, 323 (1996).
29. Souverijns, W., Verrelst, W., Vanbutsele, G., Martens, J. A., and Jacobs, P. A., *J. Chem. Soc., Chem. Commun.*, 1671 (1994).
30. Boronat, M., Viruela, P., and Corma, A., *J. Phys. Chem. B* **101**, 10069 (1997).
31. Magnoux, P., Gallet, A., and Guisnet, M., *Bul. Soc. Chim. Fr.* **5**, 810 (1987).
32. Cheng, W.-C., Peters, A. W., and Rajagopalan, K., *in* "The Hydrocarbon Chemistry of FCC Naphta Formation" (H. J. Lovink, and L. A. Pine, Eds.), p. 105. Technip, Paris, 1990.